Front. Mech. Eng. 2023, 18(1): 1
https://doi.org/10.1007/s11465-022-0717-z

RESEARCH ARTICLE

Machinability of ultrasonic vibration-assisted micro-grinding in biological bone using nanolubricant

Yuying YANG[a], Min YANG[b], Changhe LI (✉)[a], Runze LI[c], Zafar SAID[d], Hafiz Muhammad ALI[e], Shubham SHARMA (✉)[f]

[a] *School of Mechanical and Automotive Engineering, Qingdao University of Technology, Qingdao 266520, China*
[b] *College of Physics, Qingdao University, Qingdao 266071, China*
[c] *Department of Biomedical Engineering, University of Southern California, Los Angeles, CA 90089, USA*
[d] *Department of Sustainable and Renewable Energy Engineering, University of Sharjah, Sharjah 27272, United Arab Emirates*
[e] *Mechanical Engineering Department, King Fahd University of Petroleum and Minerals, Dhahran 31261, Saudi Arabia*
[f] *Department of Mechanical Engineering, IK Gujral Punjab Technical University, Jalandhar 144603, India*

✉ *Corresponding author. E-mails: sy_lichanghe@163.com (Changhe LI); shubham543sharma@gmail.com (Shubham SHARMA)*

ABSTRACT Bone grinding is an essential and vital procedure in most surgical operations. Currently, the insufficient cooling capacity of dry grinding, poor visibility of drip irrigation surgery area, and large grinding force leading to high grinding temperature are the technical bottlenecks of micro-grinding. A new micro-grinding process called ultrasonic vibration-assisted nanoparticle jet mist cooling (U-NJMC) is innovatively proposed to solve the technical problem. It combines the advantages of ultrasonic vibration (UV) and nanoparticle jet mist cooling (NJMC). Notwithstanding, the combined effect of multi parameter collaborative of U-NJMC on cooling has not been investigated. The grinding force, friction coefficient, specific grinding energy, and grinding temperature under dry, drip irrigation, UV, minimum quantity lubrication (MQL), NJMC, and U-NJMC micro-grinding were compared and analyzed. Results showed that the minimum normal grinding force and tangential grinding force of U-NJMC micro-grinding were 1.39 and 0.32 N, which were 75.1% and 82.9% less than those in dry grinding, respectively. The minimum friction coefficient and specific grinding energy were achieved using U-NJMC. Compared with dry, drip, UV, MQL, and NJMC grinding, the friction coefficient of U-NJMC was decreased by 31.3%, 17.0%, 19.0%, 9.8%, and 12.5%, respectively, and the specific grinding energy was decreased by 83.0%, 72.7%, 77.8%, 52.3%, and 64.7%, respectively. Compared with UV or NJMC alone, the grinding temperature of U-NJMC was decreased by 33.5% and 10.0%, respectively. These results showed that U-NJMC provides a novel approach for clinical surgical micro-grinding of biological bone.

KEYWORDS micro-grinding, biological bone, ultrasonic vibration (UV), nanoparticle jet mist cooling (NJMC), grinding force, grinding temperature

1 Introduction

The cross-integration of mechanical science and biomedicine has become a hot research topic. As an important component of living organisms, bone tissue plays an important role in supporting and weight-bearing [1], protecting internal organs [2], accomplishing movement [3], and participating in metabolism and hematopoiesis [4]. Due to the needs of patients with bone diseases and fracture treatment and plastic surgery, more and more attention has been paid to the cutting and treatment of bone tissue during surgery [5]. As a traditional precision machining method, grinding is increasingly being used in bone surgery to achieve the removal of bone tissue. Micro-grinding mainly refers to the use of micro-abrasives (the diameters of the abrasive shank and abrasive head are usually 3–6 and < 1 mm, respectively) [6] with a processing feature size of less than 0.05 mm to directly perform mechanical removal processing and form the desired shape [7]. It is an extension of the traditional machining process to the micro-scale. It plays an important role in the field of micromachining, with the advantages of high accuracy of the edges of machined parts and suitability for machining hard and brittle

Received February 12, 2022; accepted June 13, 2022

materials [8]. As a result, it is increasingly being used in orthopedic surgery to remove bone tissue. However, given that bone tissue is a typical anisotropic material, there are significant differences in the physical and mechanical properties in different directions [9]. Therefore, it is difficult to choose the best grinding speed that can reduce the bone temperature in actual surgery [10]. During clinical orthopedic surgical grinding, the grinding temperature of the bone material directly affects its biological activity and the degree of thermal damage to the surrounding soft tissues [11]. Mizutani et al. [12] proposed a cold air jet as cooling for bone grinding with miniature ball-end diamond wheels, which can prevent chip adhesion and stably suppress the temperature under a threshold temperature of 50 °C. However, when the temperature of the bone material in direct contact with the grinding tool reaches 47 °C and is maintained for more than 1 min, thermal necrosis will immediately occur due to high temperature [13]. Meanwhile, temperature higher than 43 °C will lead to thermal damage in the nerve tissue [14]. Thermal necrosis of bone material and surrounding soft tissues can prolong the patient's postoperative recovery time [15]. Thermal injury caused by bone grinding temperature is a bottleneck problem in surgery. Currently, saline drip irrigation is commonly used in the grinding area to remove heat by convective heat exchange, thus achieving cooling of the hot area [16]. Kondo et al. [17] found through experiments that using saline flood cooling reduced bone grinding temperature and the spread of high-temperature areas. However, this method has a low cooling efficiency. It requires a large amount of coolant dripping in the grinding area, which tends to reduce the visibility of the surgical area [18]. Meanwhile, bone tissue composition contains a certain amount of polysaccharide proteins. The viscosity of polysaccharide proteins in grinding chips is enhanced at higher grinding temperatures [19], and under the extrusion of grinding tools and bone surfaces, grinding chips adhere to the surface of grinding tools, leading to clogging of grinding tools [20]. Therefore, there is an urgent need for a new grinding process to solve such problems.

In response to the problems of insufficient cooling capacity and poor visibility in clinical surgical bone grinding, researchers proposed the minimum quantity lubrication (MQL) grinding technique [21]. In the MQL grinding process, an extremely small amount of lubricating fluid and a gas with a certain pressure are mixed and atomized and then sprayed into the grinding area for cooling and lubrication [22]. MQL grinding can effectively reduce friction and energy consumption of the workpiece surface [23], reduce wear and tear, greatly improve the working environment [24], and reduce pollution to the natural environment [25], and it is an efficient and green processing technology. However, the cooling performance of MQL high-pressure airflow is limited and cannot meet the heat transfer requirements in the high-temperature environment of the grinding zone [26]. The machining quality of the workpiece and the life of the grinding tool are still far from those of physiological saline drip grinding, and this technology still needs further development [27]. Nanoparticle jet mist cooling (NJMC) is an upgrade and optimization of MQL [28]. According to the enhanced heat transfer theory, the heat transfer capacity of solids is much better than that of liquids and gases [29]. Therefore, nanoscale solid particles are selected to make nanofluid. The nanoscale solid particles, lubricating fluid, and high-pressure gas are mixed and atomized, and sprayed into the grinding zone in the form of a jet [30]. Zhang et al. [31] fabricated nanoparticles with different concentrations of molybdenum disulfide (MoS_2), carbon nanotubes (CNTs), and their mixtures (MoS_2-CNTs). Nickel-based alloy, a difficult-to-machine workpiece material, was used to experimentally study the grinding performance in the MoS_2-CNT MQL. The results showed that the surface quality and machining accuracy of the workpiece were significantly improved due to the lubricating property and high thermal conductivity of the nanoparticles. Moreover, the grinding performance of the nanoparticles was studied by comparing the addition of MoS_2 or CNT to the MQL grinding fluid and nanoparticles without concentration. Yang et al. [32] added hydroxyapatite, silica (SiO_2), Fe_2O_3, and carbon nanotubes to physiological saline and investigated the effect of different nanoparticles on bone grinding temperature under nanoparticle jet minimum quantity cooling conditions. The results showed that the different nanoparticles had different thermophysical properties, which led to different bone surface temperatures. The nanoparticles could degrade naturally in the human body several months to a year after the end of the procedure. Their medicinal components were absorbed by the body, playing a supplementary therapeutic role. SiO_2 nanoparticles are the most typical and widely used nano-drug carriers with good biocompatibility and mechanical properties in the biomedical field. As a structurally simple nanomaterial, SiO_2 nanoparticles could introduce a variety of functional groups through surface modification, and they are widely used in biomedical fields such as drug carriers and drug release due to their good biocompatibility, high specific surface area, and chemical stability [33] (Fig. 1). The NJMC method added medical nanoscale solid particles to the lubricating fluid, which improved the proportion of heat transfer to the outside environment to a certain extent. However, the nanoparticle content was very small, and its enhanced heat transfer effect was poor and needed further improvement [34].

Given the low effective flow rate and tendency to cause clogging of grinding tools during micro-grinding, ultrasonic vibration (UV)-assisted grinding has been proposed [35]. UV-assisted grinding uses high-frequency

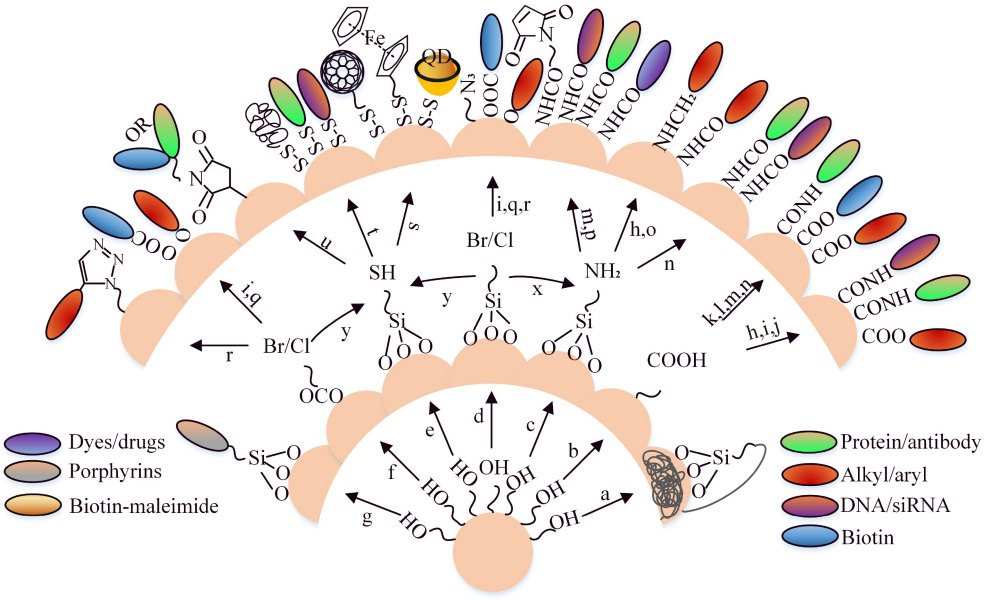

Fig. 1 Schematic of the functionalization and bio-coupling of silica nanoparticles.

impact to change the kinematic and thermodynamic properties between the grinding tool and the workpiece material to obtain superior grinding performance. UV-assisted grinding is an effective way for machining of difficult-to-cut materials [36], such as Ni-based superalloy [37], TC4 titanium alloy [38], and brittle bone materials [9]. The process is popular among researchers and clinicians due to the advantages of miniaturized equipment and high stability. Cao et al. [39] studied the vibration coupling effects and machining behavior in UV-assisted grinding of Inconel 718 Ni-based superalloy. Meanwhile, the grinding force and machined surface quality of UV-assisted grinding and conventional creep-feed grinding were compared and analyzed. The results showed that UV-assisted grinding had better grinding performance than conventional creep-feed grinding [40]. Alam et al. [41] carried out UV planar cutting of cortical bone and studied the effect of different vibration parameters on cutting forces. Gupta and Pandey [42] studied the drilling forces and torques of bone at different rotational speeds, feed rates, drill diameters, and UV amplitudes. The results showed that the rotational UV bone drilling method could minimize the forces and torques during bone drilling. Babbar et al. [43] used a hybrid cumulative equivalent minute (CEM43 °C) and Arrhenius model to compare and analyze the causes of thermal damage to human tissues during conventional grinding and UV-assisted grinding of bone materials. The study showed that UV-assisted grinding could effectively reduce the grinding force and grinding temperature, inhibit the clogging of grinding tools, and improve the quality and efficiency of workpiece grinding. UV grinding reduced the grinding temperature during bone grinding and could effectively prevent osteonecrosis and nerve damage.

UV further improved the grinding performance of MQL-assisted grinding. Li et al. [44] investigated the grinding performance of different vibration frequencies and amplitudes from the viewpoint of grinding surface quality and tool life using an experimental approach. The results showed that the best surface quality could be obtained using a high frequency (11.4 kHz) and a low feed rate. UV could extend the tool life by two times compared with conventional grinding. In addition, MQL significantly improved tool life in UV-assisted grinding. However, there was a gap between the selected parameters and the requirements to produce UV in a strict sense. Therefore, the excellent machining effect of UV may not be fully exploited. Jia et al. [45] found that the combination of multi-angle two-dimensional (2D) UV and NMQL techniques significantly reduced the adhesion and material peeling on zirconia ceramics. Rabiei et al. [46] reported that UV and NMQL compounding could reduce the grinding temperature from 254 to 132 °C without any thermal damage or burning compared with dry grinding. Yan et al. [47] experimentally investigated the effects of dry, UV, and MQL compounding processes on the turning properties of Ti–6Al–4V alloy materials. They found that the tool contact length was reduced, and the chip shape was optimized under the condition of a continuous MQL with UV system. Gao et al. [48] evaluated the surface properties of GH4169 nickel-based alloy using 2D UV-assisted grinding and NMQL coupling. The results showed that the surface roughness was reduced by 19.5% and 39.9% for both couplings compared with UV and NMQL, respectively. The kinematic model of 2D UV was also established to simulate the relative motion trajectories of the abrasive grains and the workpiece under different UV angles.

However, the current research on UV and NMQL

compounding process is mainly focused on metal, ceramic, and other materials. Research related to the micro-grinding of biological bone with complex structure and anisotropic physical and mechanical properties is lacking. Therefore, to investigate the effectiveness of ultrasonic vibration-assisted nanoparticle jet mist cooling (U-NJMC) micro-grinding in biological bone, a grinding experimental study was conducted on fresh bovine tibial dense bone, which has the most similar mechanical properties to human bone. The influence of different grinding conditions (dry grinding, drip, UV, MQL, NJMC, and U-NJMC) on the grinding performance of biological bone were designed and researched. Grinding force, grinding force ratio, friction coefficient, and grinding temperature were used as characterization parameters to study the effect of UV and NJMC on the thermal damage of micro-grinding force. The active control strategy of thermal damage of micro-grinding force was investigated to provide technical support for clinical surgery.

2 Experimental

2.1 Experimental setup

The experimental setup was a U-NJMC micro-grinding bone surgery experimental platform, which mainly included an axial UV system and an NJMC system, as shown in Fig. 2. The main technical parameters consisted mainly of a spindle power of 2.5 kW, a maximum spindle speed (n) of 24000 r/min, a workbench with dimensions of 600 mm × 1200 mm × 800 mm, an axial vibration amplitude (A) of 2–8 μm, and a frequency (f) of 18–22 kHz. In the NJMC system, the nanoparticles and saline could be uniformly distributed by UV bar. After the two were mixed in the mixing chamber and prepared into a low-concentration nanofluid, the nanofluid was ejected from the electrostatic atomization nozzle by the MQL pump. Then, the nanofluid droplets were charged and atomized by the adjustable high-voltage direct current power supply to form a cluster of charged micro-droplets, which were transported to the workpiece surface in a controlled and orderly manner driven by the electric field force and mainly played the role of lubrication and cooling in the grinding motion. The 3D grinding force dynamometer (YDM-III99, Dalian University of Technology, China) was used to measure the tangential, normal, and axial grinding force in real time, as shown in Fig. 3(a). The dynamometer is connected to the charge amplifier using the matching high-transmittance leads and to the A/D data acquisition card installed on the PC. DynoWare software was used to measure and record the grinding force. In the acquisition of grinding force data, the data collection frequency should be as high as possible, so that it can collect detailed grinding force information as much as possible. The sampling frequency of 1 kHz can obtain the best grinding force information based on equipment performance and our previous work in the laboratory [3,31]. In addition, low-pass filtering of DynoWare was used to denoise the obtained grinding force signal. Taking the center of the grinding force sampling point in the effective grinding area as the benchmark, 100 data points were selected as the basic data of the grinding force analysis. The average value was calculated to obtain the corresponding force average

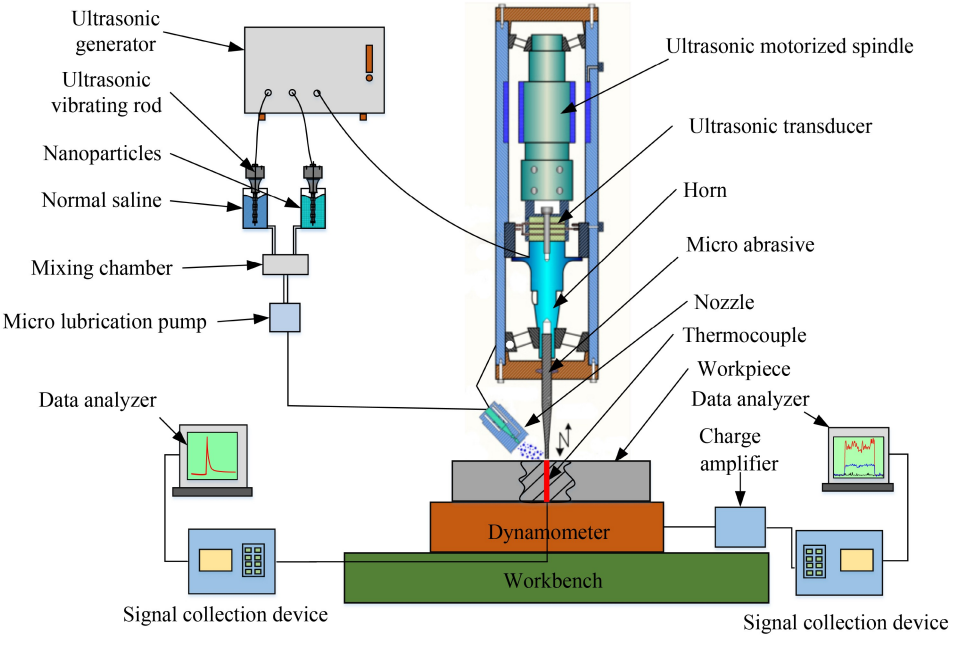

Fig. 2 Diagram of the bone micro-grinding experiment.

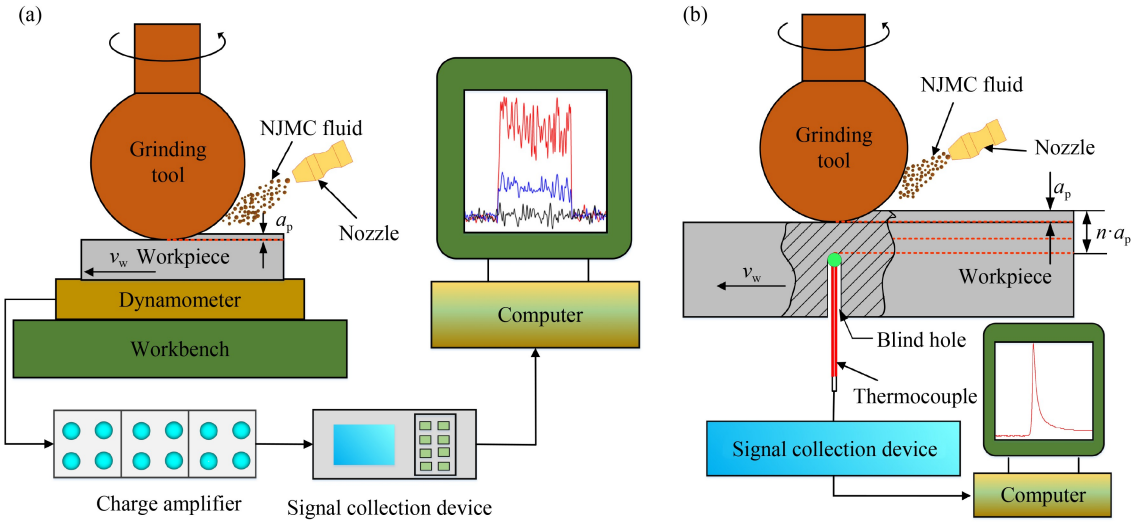

Fig. 3 Schematic of grinding measurement: (a) grinding force and (b) grinding temperature.

value. The data selection method described above ensured the representativeness of the grinding force signal. The bone grinding surface temperature was measured by the perforated buried full artificial thermocouple method. The blind hole was drilled at the central axis on the other surface of the workpiece. Under micro-grinding condition, the shallow grinding depth (a_p = 0.015 mm) easily led to the penetration of the workpiece surface when the blind hole was drilled. Thus, the distance between the bottom of blind hole and the top surface is 0.3 mm. To achieve accurate grinding temperature, the micro-grinding was executed several times at the same grinding conditions until the top surface's location moved to the bottom of the blind hole [49], as shown in Fig. 3(b).

2.2 Workpiece materials and abrasives

Because of the hard and brittle characteristics of biological bone, a diamond grinding tool with abrasive grains of 200# mesh was selected as the micro-grinding tool. The average grain size was 75 μm. The electroplated diamond micro-grinding rod with stable processing quality and good overall performance was selected. The diameter of the grinding head and tool handle was 1 and 3 mm, respectively. Given that the composition of bovine bone is basically similar to that of human bone and the physiological and mechanical properties are similar to those of human bone tissue, the dense bone in the middle of the bovine tibia was used as the experimental material in this study. Fresh bovine tibia from 2–3-year-old adult cattle purchased from a slaughterhouse was soaked in physiological saline, and the soft tissue attached to the external surface of the tibia was removed [50]. A section of the tibia with relatively uniform diameter was taken and prepared into bone samples with size of 40 mm × 10 mm × 5 mm. The samples were polished with grit sandpaper to remove any damage caused during the sample preparation process so that the surface to be processed was flat and smooth and then treated with saline. Then, the samples were used for the experiments immediately or placed in a −20 °C freezer to maintain their thermophysical properties for subsequent experiments [51]. However, all specimens were kept for a maximum of one week to avoid changes in tissue properties over time, making the experimental results non-comparable. Also, in order to ensure that the bone samples could recover their biological properties during the experiments, the bone samples to be processed in the freezer needed to be removed and placed at room temperature for 1 h to re-warm before the next experiment. Bone material is a typical anisotropic material (Fig. 4) with significant differences in physical and mechanical properties of different directions. The radial, axial, and tangential structures differ significantly, so the mechanical properties and grinding characteristics must also differ when micro-grinding is performed on different faces in different directions. For this reason, three directions (axial, radial, and tangential) of biological bones were selected to study the micro-grinding characteristics of bone tissue in different directions.

2.3 Nanoparticle materials

Saline was used as the base fluid, and SiO_2 nanoparticles were used as the nanoscale solid additive with an average particle size of 20 nm. The suspension stability of nanofluids is the best when the volume fraction is 2 vol.% [11]. Nanoparticles made the nanofluid's thermal conductivity much higher than that of liquid saline due to the excellent heat transfer properties. Moreover, the rolling effect and weak shear surface between molecular layers of nanoparticles made the nanofluid exhibit excellent tribological properties [48]. Polyethylene glycol 400 (PEG400) with a volume fraction of 1/10 was added

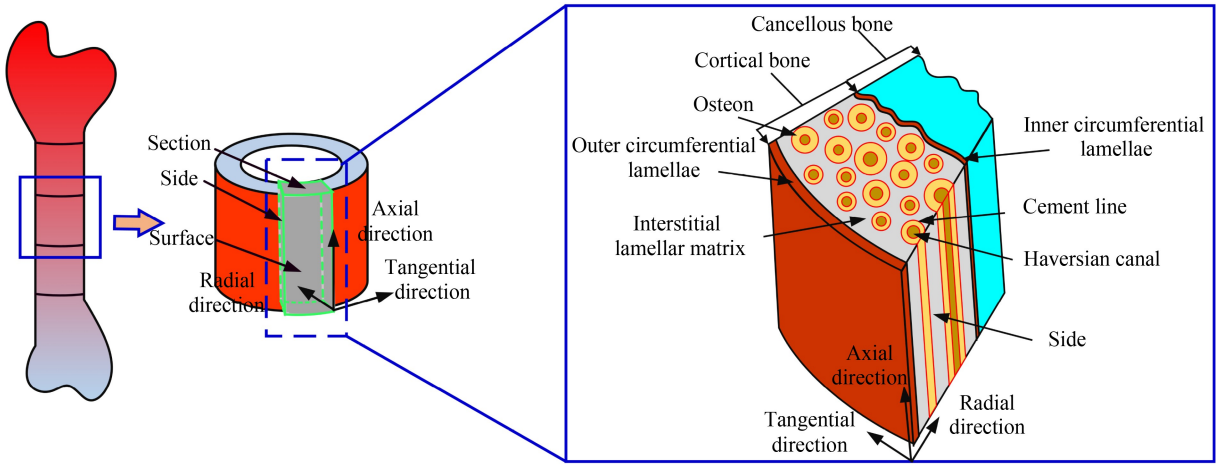

Fig. 4 Schematic of sample orientations and structure in compact bone.

as a surface dispersant and assisted with UV to improve the stability of the suspension [7]. SiO_2 nanoparticles were mixed with physiological saline to prepare a low-concentration nanofluid. The specific implementation method is as follows: First, 1.2 g of SiO_2 nanoparticles was added into 1000 mL of normal saline. Then, 2 mL of PEG400 dispersant was added. Finally, after mechanical stirring, the sample was vibrated in an ultrasonic vibrator for 15 min to make a nanofluid with good dispersion performance, and the test was carried out immediately. The nanofluid was sprayed to the bone grinding area, which guaranteed the safety to the human body and served as an auxiliary cooling function. Before starting the test, the ultrasonic generator should first be turned on. The UV would interfere with the heat generated by the workpiece grinding process at this time, so it was necessary to wait for the UV to reach a stable state before conducting the grinding experiment, which would not happen with conventional micro-grinding.

2.4 Experimental conditions

Six grinding processes, namely, dry grinding, drip irrigation, UV, MQL, NJMC, and U-NJMC, were performed to verify the performance of U-NJMC micro-grinding. Based on pre-trial experience and previous studies [52,53], drip grinding was made of physiological saline with a liquid flow rate of 50 mL/h. The nanofluid was prepared by a two-step method, and further details of this preparation method were reported in Ref. [52]. The amplitude and frequency of UV were set to 7.5 μm and 20 kHz, respectively. Further details on this testing method can also be found in Ref. [53]. The details of experimental lubrication parameters under different lubrication conditions for grinding are shown in Table 1.

In order to maintain experimental consistency, the processing parameters were kept constant except for the different lubrication conditions, as shown in Table 2.

3 Results and discussion

3.1 Effect of bone tissue orientation on grinding force

The grinding force is an important physical quantity to evaluate the material removal characteristics in the grinding process [54]. It directly affects the surface quality and damages the biological bone material, which seriously affects the healing of bone tissue after surgery. At the same time, it can also provide a basis for the wear of abrasives and facilitate the timely replacement of abrasives. To estimate the grinding force of bone tissue during micro-grinding in different directions, diamond abrasive was used, and the grinding parameters were selected as shown in Table 2. Micro-grinding was performed on the side, section, and surface. To ensure the accuracy of the measurement results, each group of parameters was measured five times, and the statistical values were taken [55]. The results of the axial, tangential, and normal grinding forces are shown in Fig. 5, where F_a, F_t, and F_n are the axial grinding force, tangential grinding force, and normal grinding force, respectively.

The results showed that F_n and F_t were the largest with 7.19 and 3.23 N, respectively, and F_a did not differ significantly when grinding the cross-section. F_n and F_t were 5.59 and 1.87 N, respectively, which decreased by 22.2% and 42.1%, respectively, with respect to the cross-section. F_n and F_t were the smallest when grinding the surface and decreased by 28.5% and 49.2% with respect to the cross-section, respectively. This was mainly because bone tissue is an anisotropic material. The dense bone can usually be considered as a fibrous toughened composite material, which was the external support tissue of the bone and consisted of osteon, interstitial lamella, circumferential lamellae, cement line, and Haversian system arranged in an axial direction. Large amounts of bone osteon and the inter-, inner, and outer

Table 1 Lubrication parameters under different lubrication conditions

No.	Lubrication conditions	Lubrication parameters
1	Dry	–
2	Drip	Liquid flow rate Q = 50 mL/h
3	UV	Axial vibration amplitude A = 7.5 μm, frequency f = 20 kHz
4	MQL	Q = 10 mL/h, air pressure P = 0.5 MPa, nozzle angle α = 45°, injection distance D = 15 mm
5	NJMC	Q = 10 mL/h, P = 0.5 MPa, α = 45°, D = 15 mm, nanofluid: 1.2 g SiO_2 + 2 mL PEG400 + 1000 mL saline
6	U-NJMC	A = 7.5 μm, f = 20 kHz, Q = 10 mL/h, P = 0.5 MPa, α = 45°, D = 15 mm, nanofluid: 1.2 g SiO_2 + 2 mL PEG400 + 1000 mL saline

Table 2 Experimental scheme of micro-grinding process

No.	Grinding process parameters	Numerical value
1	Grinding tools	Micro-grinding
2	Spindle speed n	21000 r/min
3	Feeding speed v_w	120 mm/min
4	Grinding depth a_p	0.015 mm

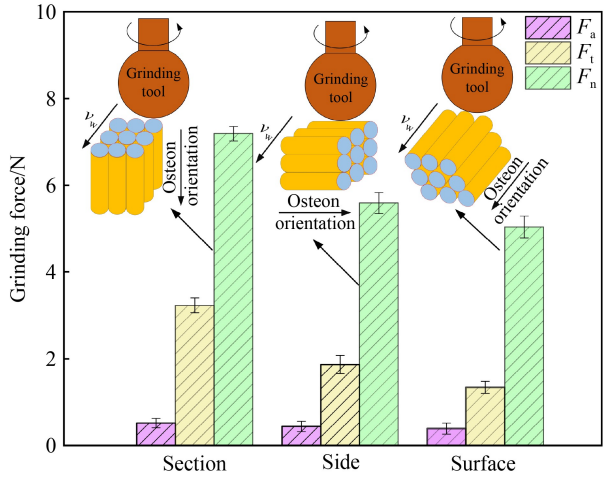

Fig. 5 Comparison of grinding force on different bone tissue orientations.

circumferential lamellae in the dense bone increase the slip resistance of the bone material during plastic deformation, exponentially increasing the energy absorption capacity and improving the fracture toughness of the bone material in the cross-section grinding process. The grinding resistance of the abrasive grains and the friction between the abrasive grains and the specimen were larger. This means that more energy needed to be accumulated to grind and propagate through the bone unit under this direction compared with the other two grinding directions. Thus, the grinding force during cross-sectional grinding was the largest, as shown in Fig. 6(a). In addition, the bone-bonding line was the weakest part of the dense bone due to the presence of the bonding line boundary around the bone unit. Under the action of the grinding force, the bone material was extremely peeled away from the bone matrix; it produced deflection and distortion along the bond line and extended into the interior of the bone material along the bond line [56]. Some microcracks turned into macroscopic cracks, which had a destructive effect on the bone unit system and affected the biological activity of the bone material and its regenerative capacity. Due to the co-existence of cracks expanding along the long axis direction of the bone unit and cracks expanding along the grinding direction, the grinding chips produced in this mode were fragmentary. When grinding the lateral side, the grinding direction was consistent with the bone unit direction, and the grinding resistance was much smaller when grinding the bone unit. The grinding direction was perpendicular to the annular bone plate direction, which was cross-sectional grinding relative to the inner and outer annular bone plate. As shown in Fig. 6(b), the grinding resistance was larger. The grinding direction was consistent with the bone unit direction and the annular bone plate direction when grinding the surface. The cutting resistance was much smaller when grinding on the bone unit and the annular bone plate. Hence, the grinding force during surface grinding was minimal, as shown in Fig. 6(c).

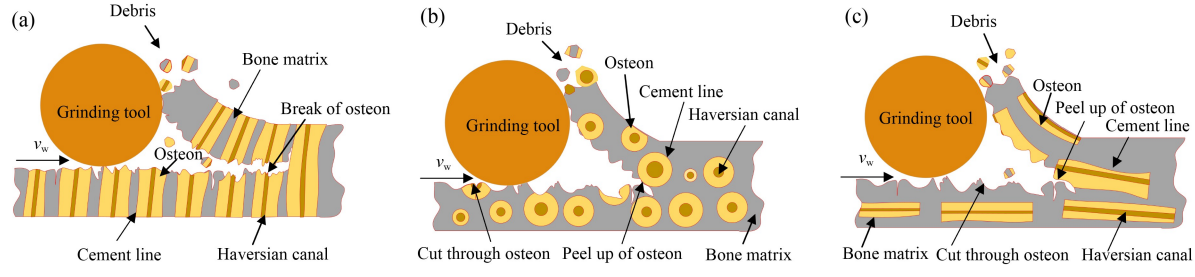

Fig. 6 Schematic of bone tissue grinding in different directions. (a) Cross grinding direction, (b) side grinding direction, and (c) surface grinding direction.

Furthermore, as the angle between the bone unit distribution and the bone long-axis direction varied between 5° and 15°, there was always an angle between the bone unit long-axis direction and the grinding direction [56]. During surface grinding, the direction of crack propagation in the grinding direction was highly susceptible to propagate upward/downward along the bond line boundary toward the interior of the material. Therefore, when the crack propagation encounters the bone unit, the crack propagation changes along the direction of the bone unit inclination rather than directly through the bone unit.

3.2 Effect of different working conditions on grinding force

The experimental research was carried out on the side of the specimen using diamond micro-abrasives to investigate the effect of different grinding conditions on the grinding force. Typical measured signals of grinding force under six different working conditions were obtained, as shown in Fig. 7. F_n and F_t of drip, MQL, UV, NJMC, and U-NJMC grinding were reduced compared with dry grinding, indicating that the use of grinding fluid or UV during the grinding process could reduce the grinding force. The grinding force obtained by U-NJMC micro-grinding was the smallest and showed certain advantages. To accurately represent the magnitude of the grinding force under various lubrication conditions, five sets of experiments were repeated under each lubrication condition, and 100 consecutive data points were intercepted in each group of grinding force stabilization phase and processed for mathematical and statistical analysis. Figure 8 shows the statistical values of the grinding force under the six lubrication conditions. F_n and F_t obtained by dry grinding were 5.59 and 1.87 N, respectively. F_n and F_t of NJMC condition were 3.41 and 0.90 N, respectively. Compared with conventional dry grinding, F_n and F_t in NJMC grinding were reduced by 39.0% and 51.9%, respectively. F_n and F_t in UV grinding were 2.62 and 0.67 N, respectively. Compared with conventional dry grinding, F_n and F_t of UV were reduced by 53.1% and 64.2%. F_n and F_t of U-NJMC were 1.39 and 0.32 N, respectively. Compared with dry grinding, U-NJMC could decrease F_n and F_t by 75.1% and 82.9%, respectively. The grinding force was the highest during the dry grinding process due to the absence of any lubricant. Drip took away the grinding chips with a large amount of grinding fluid to reduce friction, which made the grinding force lower than that in dry grinding. MQL could improve the visibility of the grinding area. Still, only a small amount of saline grinding fluid carried away the grinding chips to reduce friction, which made the trend of reducing the grinding force less obvious. The lubricating property of SiO_2 nanoparticles in NJMC reduced the friction between the grinding tool and the workpiece and decreased the grinding force, which was significantly less effective than NJMC. The lubrication effect of MQL was obviously inferior to that of NJMC as it only relied on a small layer of saline lubricating fluid in MQL grinding.

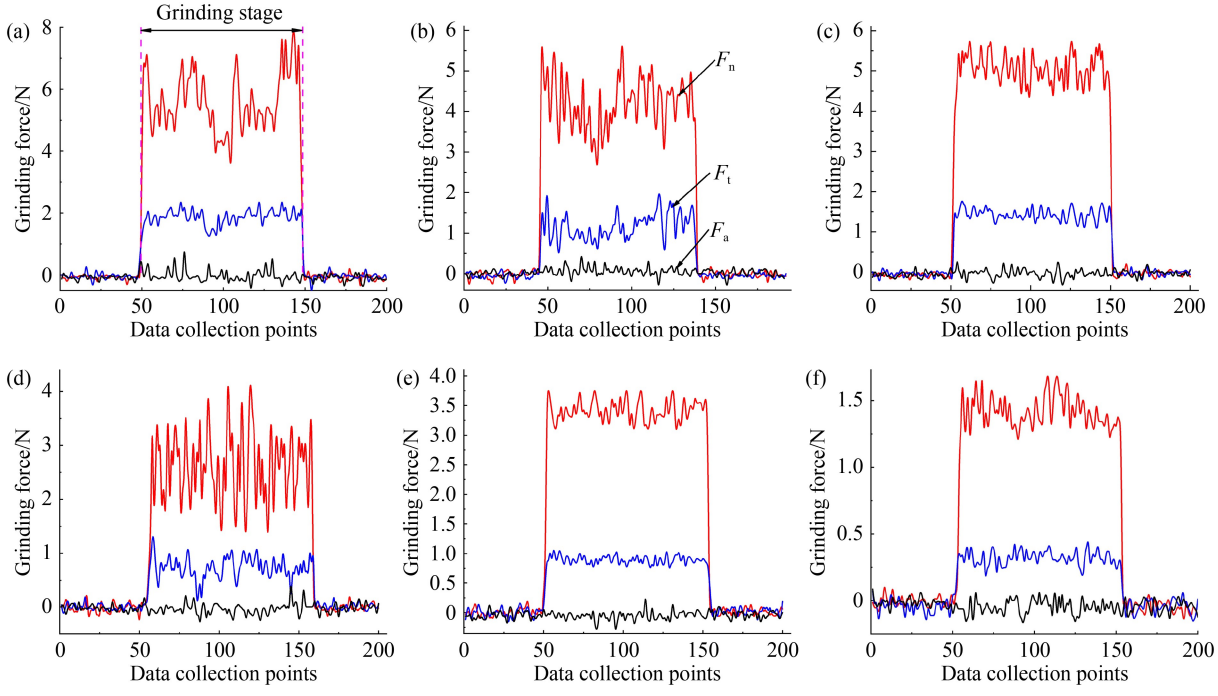

Fig. 7 Typical diagram of grinding force in different grinding conditions: (a) dry, (b) drip, (c) minimum quantity lubrication, (d) ultrasonic vibration, (e) nanoparticle jet mist cooling, and (f) ultrasonic vibration-assisted nanoparticle jet mist cooling.

The friction coefficient μ is the ratio of F_t and F_n, which can intuitively reflect the lubrication effect between the sliding interfaces in the grinding zone. The coefficient of friction μ was expressed as follows:

$$\mu = F_t / F_n. \quad (1)$$

Figure 9 shows μ under six different lubrication conditions. Dry grinding had the maximum friction coefficient ($\mu_{dry} = 0.335$). For the rest of the grinding conditions, drip, MQL, and NJMC based on water-based lubricants showed a slightly lower friction coefficient ($\mu_{drip} = 0.277$, $\mu_{MQL} = 0.284$, $\mu_{NJMC} = 0.263$), whereas the friction coefficient under UV grinding was still reduced compared with water-based lubricants. U-NJMC has the smallest μ ($\mu_{U\text{-}NJMC} = 0.230$) among all grinding conditions. Compared with dry, drip, MQL, UV, and NJMC grinding, the U-NJMC condition friction coefficient was reduced by 31.3%, 17.0%, 19.0%, 9.8%, and 12.5%, respectively.

In addition to the grinding force and friction coefficient, the specific grinding energy e_s is the most common parameter to evaluate the grinding performance. It refers to the total system energy consumed per unit time for grinding to remove a unit volume of workpiece material. It also reflects the lubrication effect of the grinding/workpiece interface. The smaller e_s is, the better the lubrication effect will be. e_s was expressed as follows [57,58]:

$$e_s = \frac{F_t \cdot v_s}{v_w \cdot a_p \cdot b_w}, \quad (2)$$

where v_s is the grinding tool linear speed, and b_w is the micro-grinding workpiece width (Fig. 10) and could be expressed as follows:

$$b_w = 2\sqrt{r^2 - (r - a_p)^2}, \quad (3)$$

where r is the radius of the abrasive.

Figure 11 shows e_s under six different grinding conditions. Dry grinding consumes the most energy, and e_s was as high as 2.47×10^4 J/mm^3, which increased F_t and generated more energy consumption. U-NJMC grinding consumed the least energy, and e_s was 0.42×10^4 J/mm^3. Compared with dry, drip, MQL, UV, and

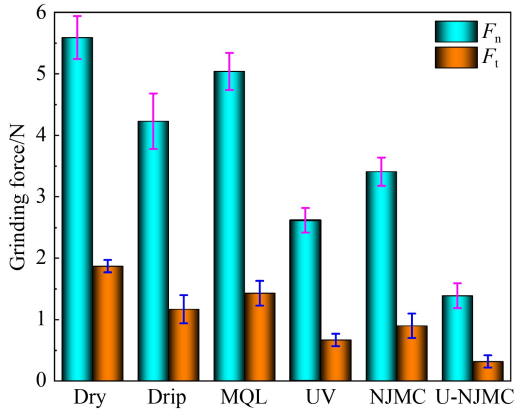

Fig. 8 Grinding force of different grinding conditions. MQL: minimum quantity lubrication, UV: ultrasonic vibration, NJMC: nanoparticle jet mist cooling, U-NJMC: ultrasonic vibration-assisted nanoparticle jet mist cooling.

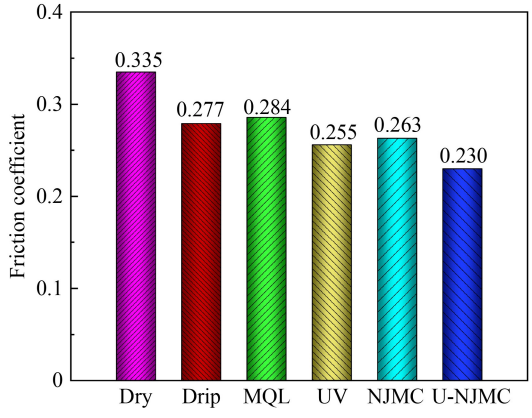

Fig. 9 Friction coefficient in different grinding conditions. MQL: minimum quantity lubrication, UV: ultrasonic vibration, NJMC: nanoparticle jet mist cooling, U-NJMC: ultrasonic vibration-assisted nanoparticle jet mist cooling.

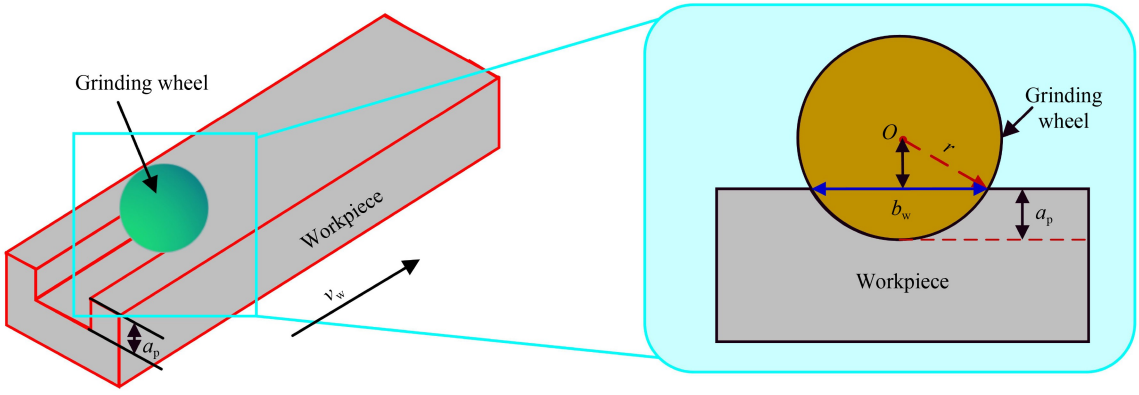

Fig. 10 Schematic of the bone grinding width.

NJMC-assisted micro-grinding conditions, e_s in U-NJMC grinding decreased by 83.0%, 72.7%, 77.8%, 52.3%, and 64.7%, respectively. The reason for the larger e_s corresponding to drip cooling lubrication compared with the U-NJMC process was that the high fluid dynamic pressure in the grinding zone prevented the water-based grinding fluid from entering the grinding zone, resulting in insufficient lubrication at the grinding tool/workpiece interface, which made the grinding force larger, thereby consuming more energy. In the case of NJMC, under the action and the penetration of the capillary network in the grinding area, the nanoparticles entered the grinding area well, which made the grinding tool/workpiece interface fully lubricated and reduced the grinding force, resulting in a reduction of the energy consumed.

3.3 Grinding temperature

In the process of bone micro-grinding, human tissue might suffer not only from mechanical damage caused by direct contact with the grinding tool or vibration during grinding but also from thermal damage caused by grinding. Most of the energy consumed by the mutual collision between the abrasive grains and the bone material was converted into heat energy and collected in the grinding zone during bone grinding. Excessive grinding temperature could easily lead to thermal damage of bone cells. Therefore, the grinding temperature under different working conditions was investigated. Figure 12 shows the grinding temperature under the six cooling conditions. The grinding temperature of dry grinding was the highest, with a peak of about 43.6 °C. The peak grinding temperature of UV-assisted micro-grinding was 4.2 °C lower than that of dry grinding. During UV-assisted micro-grinding process, the coolant was easier to pump into the grinding zone with high-frequency, alternating positive and negative hydraulic shock waves, which accelerated the renewal of coolant in the grinding zone and made the grinding temperature in the grinding zone lower. At the same flow rate, the temperature peaks of the two MQL cooling methods without UV were 5.7–14.5 °C lower than those of the dry grinding condition due to the cooling and lubricating characteristics of the grinding fluid. However, compared with drip cooling, the effect was less obvious, but it could also transfer and take away some heat to achieve the cooling effect. The peak temperature of MQL grinding was 37.9 °C, whereas that of NJMC was 29.1 °C. Under the NJMC and MQL grinding process, the concentration of grinding fluid was the same, and the main reason for the grinding temperature difference was that the thermal conductivity of solid nanoparticles was greater than that of liquid nanoparticles. Therefore, the peak grinding temperature of NJMC was lower than that of MQL, which was mainly due to the high specific surface and

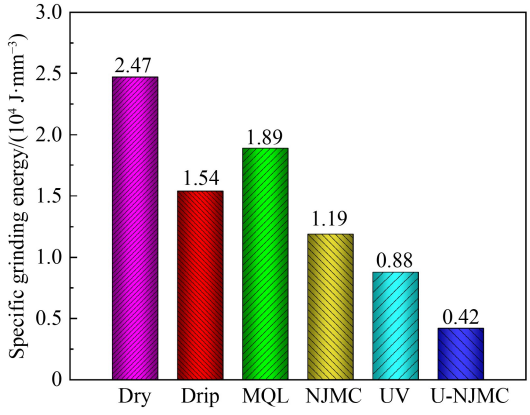

Fig. 11 Specific grinding performance under different lubrication conditions.

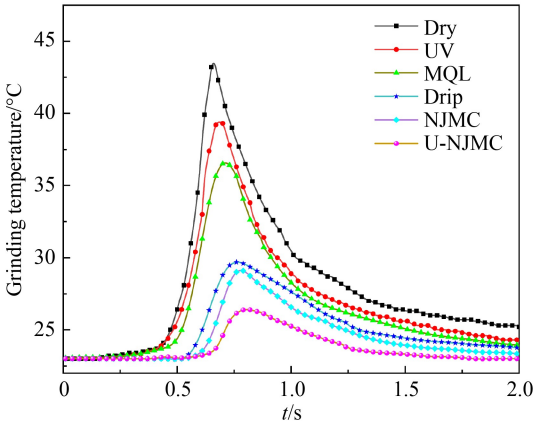

Fig. 12 Grinding temperature under different lubrication conditions.

heat capacity of nanoparticles that enhanced convective heat transfer and tribological properties in the grinding zone. U-NJMC had the lowest grinding temperature with a peak of about 26.2 °C. Compared with UV and NJMC alone, the grinding temperature of U-NJMC was reduced by 33.5% and 10.0%, respectively. This indicated that the coolant in the grinding zone accelerated the renewal under the combined action of UV and NJMC grinding fluid. Consequently, this technology greatly enhanced the convective heat transfer capacity of the cooling medium and significantly reduced the grinding temperature in the grinding zone of the machining process. Finally, the experimental findings for different grinding conditions with the corresponding grinding force (F_n and F_t), coefficient of friction (μ), specific grinding energy (e_s), and grinding temperature (T) are summarized in Table 3.

Combined with the above experimental results, the grinding heat could not be dissipated in time due to the low thermal conductivity and thermal diffusivity of the bovine tibia material. It resulted in a gradual increase in grinding temperature, which in turn caused thermal necrosis of bone cells and loss of regeneration ability.

The heat exchange capacity of the cooling medium in the confined space of the bovine tibia/micro-grinding tool was insufficient because of the lack of cooling and lubricating medium involved in the material removal process due to dry grinding. This resulted in a sharp increase in the micro-grinding temperature of the bovine tibia, which led to local water loss in the bone material and increased friction [59]. Therefore, biological bone dry grinding had poor processing performance and was prone to affect the biological activity of surrounding tissues, which triggered thermal damage to bone cells, nerves, and blood vessels around the grinding area, affecting the postoperative recovery of patients. Although a large amount of grinding fluid was involved in the grinding process in physiological saline drip micro-grinding, the low supply pressure and low initial kinetic energy made it difficult to break through the air barrier around the high-speed rotating grinding tool, which made its effective utilization rate into the grinding area low and only provided effective cooling and lubrication to the areas near the sides of the grinding tool. Moreover, diamond abrasive grains are often used as surgical grinding tools. Diamond has hydrophobic characteristics, which is even more unfavorable for saline injection into the grinding zone.

The grinding force of UV-assisted micro-grinding was lower than that of dry grinding mainly due to the cyclic reciprocation of UV frequency during UV-assisted grinding to achieve high-frequency intermittent grinding, whose schematic of UV-assisted micro-grinding is shown in Fig. 13 [60]. Given that the number of separations was the same as the frequency, the periodicity of UV caused the tool and the workpiece to separate periodically, and the coefficient of friction was greatly reduced at the moment of the appearance of the gap in the UV process, thus reducing the average friction between the tool and the material.

Table 3 Summary of micro-grinding biological bone at different lubrication conditions with the corresponding experimental results

Working conditions	F_n/N	F_t/N	μ	e_s/(J·mm^{-3})	T/°C
Dry	5.59	1.87	0.335	2.47×10^4	43.6
Drip	4.23	1.17	0.277	1.54×10^4	29.8
UV	2.62	0.20	0.284	0.88×10^4	39.4
MQL	5.04	1.43	0.255	1.89×10^4	37.9
NJMC	3.41	0.23	0.263	1.19×10^4	29.1
U-NJMC	1.39	0.32	0.230	0.42×10^4	26.2

In normal grinding, the thickness of the undeformed chip of a single abrasive grain (a_g) is calculated as follows [61]:

$$a_g = \sqrt{\frac{\pi a_p v_w}{4 v_s l_1 C \tan\theta}}, \tag{4}$$

where l_1 is the contact arc length between the grinding rod and the workpiece material, C is the effective number of abrasive grains per unit area, and θ is the average cone half angle of the abrasive grains.

In normal grinding, l_1 of a single abrasive grain is related to a_p and the abrasive diameter d_s [62]:

$$l_1 = \sqrt{a_p d_s}. \tag{5}$$

The UV changed the cutting path length of a single abrasive grain during UV-assisted micro-grinding. Therefore, the contact arc length between the grinding rod and the workpiece material in UV-assisted micro-grinding (l_2), which can be expressed as follows [62]:

$$\begin{aligned} l_2 &= \int_0^{l_1} \sqrt{1 + \left(\frac{\mathrm{d}y}{\mathrm{d}x}\right)^2}\,\mathrm{d}x \\ &= \int_0^{l_1} \sqrt{1 + \left(\frac{2\pi A f}{v_s + v_w}\cos\left(\frac{2\pi f}{v_s + v_w}x + \varphi\right)\right)^2}\,\mathrm{d}x, \end{aligned} \tag{6}$$

where φ is the initial phase of UV, and φ is usually taken

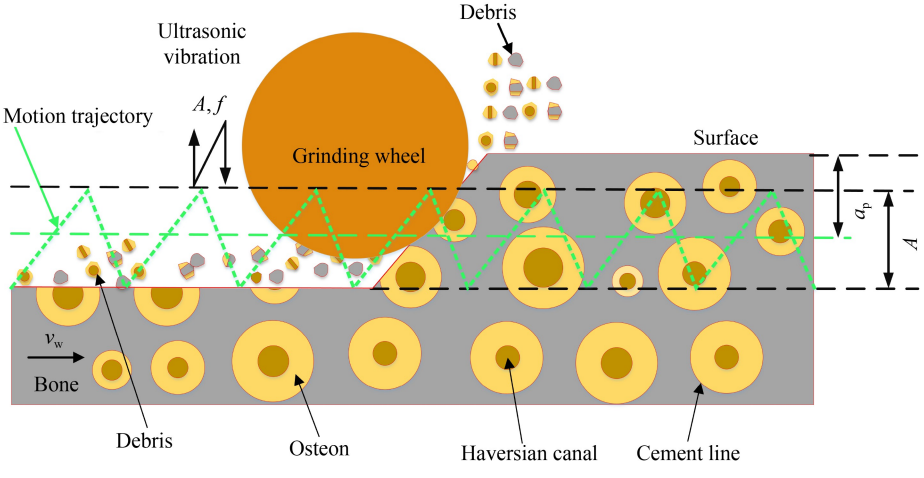

Fig. 13 Schematic of UV-assisted micro-grinding.

as 0. If l_2 is used instead of l_1 in Eq. (5), the undeformed chip thickness of UV-assisted micro-grinding is the thickness of the abrasive grain. Given that $l_2 > l_1$, UV reduced the undeformed chip thickness of a single grinding grain during grinding, which in turn made the grinding force of UV-assisted micro-grinding smaller than the normal grinding force. Furthermore, based on the vacuolar flow, stress wave, and impact kinetics theories, the abrasive tool of UV also produced cavitation and pumping effects at the abrasive tool/bone grinding interface. Microstructural damage, such as hydrogen bond breaking, occurred especially in high-protein and collagen tissues during ultrasonic high-frequency impact [63]. This process was often accompanied by heat generation, which accelerated the local liquefaction of biological tissue. The cavitation effect generated by the ultrasonic impact, which occurred mainly in the cutting process of relatively soft tissues such as fat, assisted the ultrasonic cutting effect [64].

The cavitation effect also helped to protect the surrounding tissues and reduced the surrounding tissue additional damage [65]. In addition, the cavitation effect of UV increased the self-cleaning of abrasives and enhanced the heat transfer capability of coolants. The pumping effect made it easier for medical coolant to enter the grinding zone and promoted the circulation of coolant in the grinding zone. In summary, UV softened the workpiece and changed the grinding properties of the workpiece, resulting in a reduction in the undeformed thickness during grinding. By contrast, the introduction of UV reduced the friction coefficient between the workpiece and the abrasive grains, decreasing the friction force and thus making the overall grinding force lower [66].

NJMC lubrication conditions had the participation of SiO_2 nanoparticles. The incorporation of nanoparticles provided excellent wear reduction and anti-friction effect on NJMC grinding, which was mainly related to its laminar molecular structure. As shown in Fig. 14, there were three types of hydroxyl groups on the surface of SiO_2 nanoparticles: undisturbed isolated hydroxyl groups, conjoined hydroxyl groups forming hydrogen bonds with each other, and twin hydroxyl groups with two hydroxyl groups attached to one silicon atom. The Si−O activity in the molecular structure of SiO_2 nanoparticle was related to the position it occupies. At the center of the structure, the Si−O bond was polar and had a high binding capacity. The Si−O bonds that were at the surface of the particles were highly active and capable of force binding interactions with other molecules. Figure 15 shows the lubrication mechanism of SiO_2 nanoparticles [60]. In the micro-grinding process, the uniformly dispersed spherical SiO_2 nanoparticles can play the role of "bearing-like rolling" between the friction pairs in a certain load range. In other words, the friction coefficient was reduced by changing the sliding friction into rolling friction, as shown in Fig. 15(a). Under the action of compressive and tangential stresses in the grinding process, SiO_2 nanoparticles with high surface activity were strongly chemisorbed on the workpiece grinding surface through hydroxyl groups, forming a solid SiO_2 lubricant film, as shown in Fig. 15(b). Nanoparticles had a larger specific surface area due to their small particle size, with an average particle size of 20 nm, which was tens or even thousands of micron-sized particles. Such a high specific surface resulted in an increased number of atoms on the surface. At the same time, the surface energy increased rapidly. Due to the increased number of surface atoms, the unsaturation of atomic coordination led to large numbers of unsaturated bonds and suspension bonds, making nanoparticles have high activity and large extremely unstable surface energy. As shown in Fig. 15(c), the nanoparticles formed a lubricating layer on the workpiece surface by diffusion and penetration. When the load increased, the nanoparticles reacted chemically under the action of frictional heat and formed a chemically reactive film on the frictional surface, thus enhancing the Brownian motion, prompting the fluid to break away from the bone surface faster and intensifying the heat transfer by increasing the perturbation of the boundary layer [67]. This made the grinding temperature decrease. However, the number of particles increased as the volume fraction increased. The closer the particles

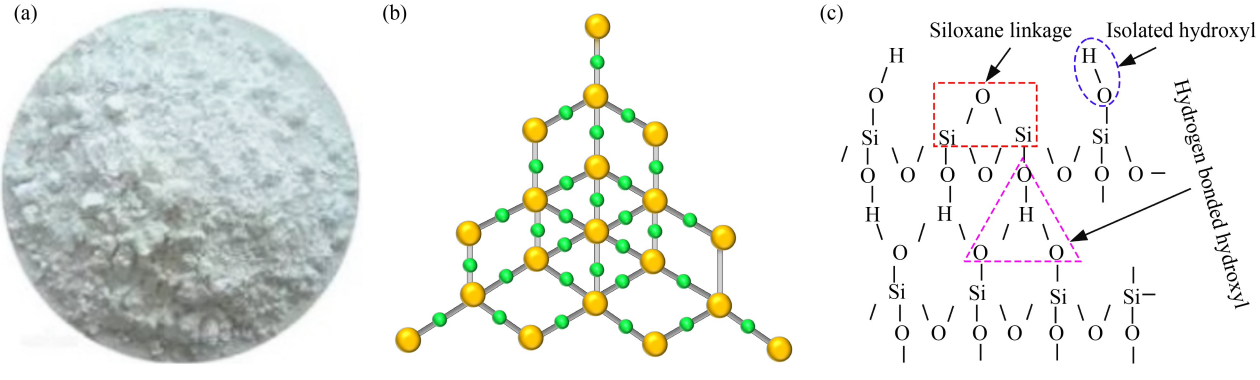

Fig. 14 Nano-SiO_2: (a) macroscopic morphology, (b) molecular structure, and (c) 3D chain structure.

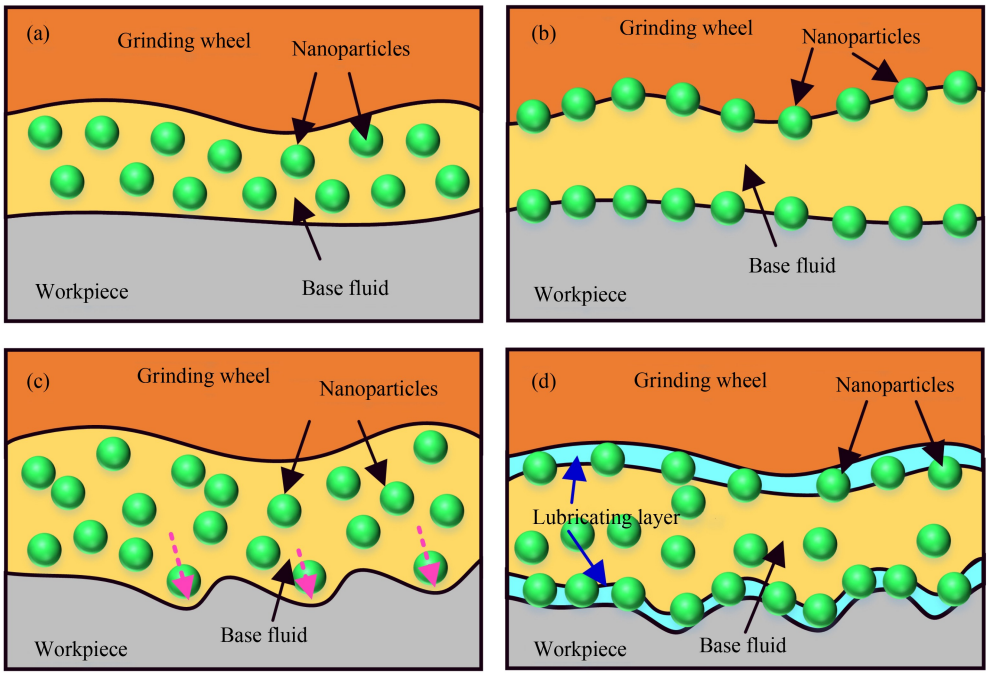

Fig. 15 Lubrication mechanism of SiO_2 nanoparticles: (a) micro-bearing action, (b) deposition membrane effect, (c) penetration and frictional chemical reactions, and (d) self-repair mechanism.

were to each other, the greater the interaction, which led to the enhanced random motion of nanoparticles. The heat exchange rate and energy transfer within the nanofluid were enhanced, which strengthened the heat transfer characteristics of the nanofluid. At the same time, the nanoparticles would gather and fill the pits formed on the surface of the friction subsets, which improved the lubrication performance between the friction subsets, thus enhancing the lubrication effect in the grinding zone, as shown in Fig. 15(d). Therefore, U-NJMC could effectively solve the high grinding force and grinding temperature of biological bone micro-grinding and provided a new way for clinical surgical cranial micro-grinding.

4 Conclusions

Grinding experiments were performed under six different working conditions: dry, drip, UV, MQL, NJMC, and U-NJMC. The grinding force, coefficient of friction, specific grinding energy, and grinding temperature were measured and compared. The following conclusions were obtained:

(1) The grinding force differs in different directions under the process of biological bone micro-grinding. The section grinding force was the largest, followed by the side grinding force. The surface grinding force was the smallest, and F_n and F_t decreased by 28.5% and 49.2% with respect to the cross-section, respectively.

(2) Compared with dry grinding, the grinding temperature of UV-assisted micro-grinding was reduced by 9.6%, and that of NJMC micro-grinding was reduced by 33.3%. F_n and F_t of UV-assisted micro-grinding were 2.62 and 0.67 N, which were reduced by 53.1% and 64.2%, respectively. Compared with dry grinding, F_n and F_t of NJMC micro-grinding were 3.41 and 0.90 N, which were reduced by 39.0% and 51.9%, respectively. Compared with dry, drip irrigation, MQL, UV, and NJMC conditions, the friction coefficient of U-NJMC condition was reduced by 31.3%, 17.0%, 19.0%, 9.8%, and 12.5%, respectively.

(3) Experiments of biological bone micro-grinding under six grinding conditions (dry, drip, UV, MQL, NJMC, and U-NJMC) were carried out. The results showed that U-NJMC obtained an F_t of 0.32 N, F_n of 1.39 N, friction coefficient of 0.230, and grinding specific energy of 0.42×10^4 J/mm^3, which provides a new technical reference for the application of micro-grinding technology in orthopedic surgery.

Nomenclature

Abbreviations

2D	Two-dimensional
CNT	Carbon nanotube
MQL	Minimum quantity lubrication
NJMC	Nanoparticle jet mist cooling
PEG400	Polyethylene glycol 400

U-NJMC	Ultrasonic vibration-assisted nanoparticle jet mist cooling
UV	Ultrasonic vibration

Variables

a_g	Thickness of the undeformed chip
a_p	Grinding depth
A	Axial vibration amplitude
b_w	Micro-grinding workpiece width
C	Effective number of abrasive grains per unit area
D	Injection distance
e_s	Specific grinding energy
f	Frequency
F_a	Axial grinding force
F_n	Normal grinding force
F_t	Tangential grinding force
l_1	Contact arc length between the grinding rod and the workpiece material in normal grinding
l_2	Contact arc length between the grinding rod and the workpiece material in UV-assisted micro-grinding
n	Spindle speed
P	Air pressure
Q	Liquid flow rate
r	Radius of the abrasive
T	Grinding temperature
v_s	Grinding tool linear speed
v_w	Feeding speed
α	Nozzle angle
μ	Coefficient of friction
μ_{dry}, μ_{drip}, μ_{MQL}, μ_{NJMC}, μ_{UV}, and $\mu_{U\text{-}NJMC}$	Friction coefficients of dry, drip, MQL, NJMC, UV, and U-NJMC grinding, respectively
θ	Average cone half angle of the abrasive grains
φ	Initial phase of ultrasonic vibration

Acknowledgement This study was financially supported by the National Natural Science Foundation of China (Grant Nos. 51905289 and 51975305), the National Key R&D Program of China (Grant No. 2020YFB2010500), the Natural Science Foundation of Shandong Province, China (Grant Nos. ZR2022QE159, ZR2020KE027, ZR2020ME158, and ZR2019PEE008), the China Postdoctoral Science Foundation (Grant No. 2021M701810), the Innovation Talent Supporting Program for Postdoctoral Fellows of Shandong Province, China (Grant No. SDBX2020012), and the Qingdao Postdoctoral Researchers Applied Research Project Funding, China (Grant No. A2020-072).

References

1. Liao Z R, Axinte D A, Gao D. A novel cutting tool design to avoid surface damage in bone machining. International Journal of Machine Tools and Manufacture, 2017, 116: 52–59
2. Robles-Linares J A, Axinte D, Liao Z R, Gameros A. Machining-induced thermal damage in cortical bone: necrosis and micro-mechanical integrity. Materials & Design, 2021, 197: 109215
3. Yang M, Li C H, Zhang Y B, Jia D Z, Zhang X P, Li R Z. A new model for predicting neurosurgery skull bone grinding temperature field. Journal of Mechanical Engineering, 2018, 54(23): 215–222 (in Chinese)
4. Conward M, Samuel J. Machining characteristics of the haversian and plexiform components of bovine cortical bone. Journal of the Mechanical Behavior of Biomedical Materials, 2016, 60: 525–534
5. Liao Z R, Axinte D, Gao D. On modelling of cutting force and temperature in bone milling. Journal of Materials Processing Technology, 2019, 266: 627–638
6. Li W, Chen Q D, Ren Y H, Jiao Y, Ibrahim A M M. Hybrid micro-grinding process for manufacturing meso/micro-structures on monocrystalline silicon. Materials and Manufacturing Processes, 2021, 36(1): 17–26
7. Yang M, Li C H, Luo L, Li R Z, Long Y Z. Predictive model of convective heat transfer coefficient in bone micro-grinding using nanofluid aerosol cooling. International Communications in Heat and Mass Transfer, 2021, 125: 105317
8. Gao S, Huang H. Recent advances in micro- and nano-machining technologies. Frontiers of Mechanical Engineering, 2017, 12(1): 18–32
9. Zhang Y, Robles-Linares J A, Chen L, Liao Z R, Shih A J, Wang C Y. Advances in machining of hard tissues—from material removal mechanism to tooling solutions. International Journal of Machine Tools and Manufacture, 2022, 172: 103838
10. Chen J J, Yuan D D, Jiang H F, Zhang L Y, Yang Y, Fu Y C, Qian N, Jiang F. Thermal management of bone drilling based on rotating heat pipe. Energies, 2022, 15(1): 35
11. Yang M, Li C H, Said Z, Zhang Y B, Li R Z, Debnath S, Ali H M, Gao T, Long Y Z. Semiempirical heat flux model of hard-brittle bone material in ductile microgrinding. Journal of Manufacturing Processes, 2021, 71: 501–514
12. Mizutani T, Satake U, Enomoto T. A study on a cooling method for bone grinding using diamond bur for minimally invasive surgeries. Precision Engineering, 2021, 70: 155–163
13. Shu L M, Li S H, Terashima M, Bai W, Hanami T, Hasegawa R, Sugita N. A novel self-centring drill bit design for low-trauma bone drilling. International Journal of Machine Tools and Manufacture, 2020, 154: 103568
14. Gholampour S, Droessler J, Frim D. The role of operating variables in improving the performance of skull base grinding. Neurosurgical Review, 2022, 45(3): 2431–2440
15. Axinte D, Guo Y B, Liao Z R, Shih A J, M'Saoubi R, Sugita N. Machining of biocompatible materials—recent advances. CIRP Annals, 2019, 68(2): 629–652
16. Li S H, Shu L M, Kizaki T, Bai W, Terashima M, Sugita N. Cortical bone drilling: a time series experimental analysis of thermal characteristics. Journal of Manufacturing Processes, 2021, 64: 606–619
17. Kondo S, Okada Y, Iseki H, Hori T, Takakura K, Kobayashi A, Nagata H. Thermological study of drilling bone tissue with a

high-speed drill. Neurosurgery, 2000, 46(5): 1162–1168
18. Kitahama Y, Shizuka H, Kimura R, Suzuki T, Ohara Y, Miyake H, Sakai K. Fluid lubrication and cooling effects in diamond grinding of human iliac bone. Medicina, 2021, 57(1): 71–80
19. Kong D Y, Lin G M, Shi Y B, Gu Z L, Gao Y, Feng Y H. Performance of heterotopic bone elicited with bone morphogenic protein-2 microspheres as a bone repair material. Materials & Design, 2020, 191: 108657
20. Novitskaya E, Chen P Y, Lee S, Castro-Ceseña A, Hirata G, Lubarda V A, McKittrick J. Anisotropy in the compressive mechanical properties of bovine cortical bone and the mineral and protein constituents. Acta Biomaterialia, 2011, 7(8): 3170–3177
21. Zhang X P, Li C H, Zhang Y B, Wang Y G, Li B K, Yang M, Guo S M, Liu G T, Zhang N Q. Lubricating property of MQL grinding of Al_2O_3/SiC mixed nanofluid with different particle sizes and microtopography analysis by cross-correlation. Precision Engineering, 2017, 47: 532–545
22. Li C H, Li J Y, Wang S, Zhang Q. Modeling and numerical simulation of the grinding temperature field with nanoparticle jet of MQL. Advances in Mechanical Engineering, 2013, 5: 986984
23. Jia D Z, Zhang N Q, Liu B, Zhou Z M, Wang X P, Zhang Y B, Mao C, Li C H. Particle size distribution characteristics of electrostatic minimum quantity lubrication and grinding surface quality evaluation. Diamond & Abrasives Engineering, 2021, 41(3): 89–95 (in Chinese)
24. Cui X, Li C H, Ding W F, Chen Y, Mao C, Xu X F, Liu B, Wang D Z, Li H N, Zhang Y B, Said Z, Debnath S, Jamil M, Ali H M, Sharma S. Minimum quantity lubrication machining of aeronautical materials using carbon group nanolubricant: from mechanisms to application. Chinese Journal of Aeronautics, 2022, 35(11): 85–112
25. Qu S S, Gong Y D, Yang Y Y, Sun Y, Wen X L, Qi Y. Investigating minimum quantity lubrication in unidirectional C_f/SiC composite grinding. Ceramics International, 2020, 46(3): 3582–3591
26. Wang X M, Li C H, Zhang Y B, Said Z, Debnath S, Sharma S, Yang M, Gao T. Influence of texture shape and arrangement on nanofluid minimum quantity lubrication turning. The International Journal of Advanced Manufacturing Technology, 2022, 119(1): 631–646
27. Gao T, Zhang Y B, Li C H, Wang Y Q, Chen Y, An Q L, Zhang S, Li H N, Cao H J, Ali H M, Zhou Z M, Sharma S. Fiber-reinforced composites in milling and grinding: machining bottlenecks and advanced strategies. Frontiers of Mechanical Engineering, 2022, 17(2): 24
28. Zhang Y B, Li H N, Li C H, Huang C Z, Ali H M, Xu X F, Mao C, Ding W F, Cui X, Yang M, Yu T B, Jamil M, Gupta M K, Jia D Z, Said Z. Nano-enhanced biolubricant in sustainable manufacturing: from processability to mechanisms. Friction, 2022, 10: 803–841
29. Liu M Z, Li C H, Zhang Y B, An Q L, Yang M, Gao T, Mao C, Liu B, Cao H J, Xu X F, Said Z, Debnath S, Jamil M, Ali H M, Sharma S. Cryogenic minimum quantity lubrication machining: from mechanism to application. Frontiers of Mechanical Engineering, 2021, 16(4): 649–697
30. Qu S S, Yao P, Gong Y D, Chu D K, Yang Y Y, Li C W, Wang Z L, Zhang X P, Hou Y. Environmentally friendly grinding of C/SiCs using carbon nanofluid minimum quantity lubrication technology. Journal of Cleaner Production, 2022, 366: 132898
31. Zhang Y B, Li C H, Jia D Z, Li B K, Wang Y G, Yang M, Hou Y L, Zhang X W. Experimental study on the effect of nanoparticle concentration on the lubricating property of nanofluids for MQL grinding of Ni-based alloy. Journal of Materials Processing Technology, 2016, 232: 100–115
32. Yang M, Li C H, Zhang Y B, Jia D Z, Zhang X P, Hou Y L, Li R Z, Wang J. Maximum undeformed equivalent chip thickness for ductile-brittle transition of zirconia ceramics under different lubrication conditions. International Journal of Machine Tools and Manufacture, 2017, 122: 55–65
33. Lin Z T, Wu Y B, Bi Y G. Rapid synthesis of SiO_2 by ultrasonic-assisted Stober method as controlled and pH-sensitive drug delivery. Journal of Nanoparticle Research, 2018, 20(11): 304
34. Biju V. Chemical modifications and bioconjugate reactions of nanomaterials for sensing, imaging, drug delivery and therapy. Chemical Society Reviews, 2014, 43(3): 744–764
35. Yuan J L, Lyu B H, Hang W, Deng Q F. Review on the progress of ultra-precision machining technologies. Frontiers of Mechanical Engineering, 2017, 12(2): 158–180
36. Cao Y, Yin J F, Ding W F, Xu J H. Alumina abrasive wheel wear in ultrasonic vibration-assisted creep-feed grinding of Inconel 718 nickel-based superalloy. Journal of Materials Processing Technology, 2021, 297: 117241
37. Miao Q, Ding W F, Xu J H, Cao L J, Wang H C, Yin Z, Dai C W, Kuang W J. Creep feed grinding induced gradient microstructures in the superficial layer of turbine blade root of single crystal nickel-based superalloy. International Journal of Extreme Manufacturing, 2021, 3(4): 045102
38. Yin G Q, Wang J H, Guan Y Y, Wang D, Sun Y. The prediction model and experimental research of grinding surface roughness based on AE signal. The International Journal of Advanced Manufacturing Technology, 2022, 120(9): 6693–6705
39. Cao Y, Zhu Y J, Ding W F, Qiu Y T, Wang L F, Xu J H. Vibration coupling effects and machining behavior of ultrasonic vibration plate device for creep-feed grinding of Inconel 718 nickel-based superalloy. Chinese Journal of Aeronautics, 2022, 35(2): 332–345
40. Kuang W J, Miao Q, Ding W F, Zhao Y J, Zhao B, Wen X B, Li S P. Fretting wear behaviour of machined layer of nickel-based superalloy produced by creep-feed profile grinding. Chinese Journal of Aeronautics, 2022, 35(10): 401–411
41. Alam K, Ghodsi M, Al-Shabibi A, Silberschmidt V. Experimental study on the effect of point angle on force and temperature in ultrasonically assisted bone drilling. Journal of Medical and Biological Engineering, 2018, 38(2): 236–243
42. Gupta V, Pandey P M. An *in-vitro* study of cutting force and torque during rotary ultrasonic bone drilling. Proceedings of the Institution of Mechanical Engineers, Part B: Journal of Engineering Manufacture, 2018, 232(9): 1549–1560
43. Babbar A, Jain V, Gupta D. Thermogenesis mitigation using ultrasonic actuation during bone grinding: a hybrid approach using CEM43°C and Arrhenius model. Journal of the Brazilian Society of Mechanical Sciences and Engineering, 2019, 41(10): 401
44. Li K M, Hu Y M, Yang Z Y, Chen M Y. Experimental study on vibration-assisted grinding. Journal of Manufacturing Science and

Engineering, 2012, 134(4): 041009

45. Jia D Z, Li C H, Zhang Y B, Yang M, Zhang X P, Li R Z, Ji H J. Experimental evaluation of surface topographies of NMQL grinding ZrO_2 ceramics combining multiangle ultrasonic vibration. The International Journal of Advanced Manufacturing Technology, 2019, 100(1): 457–473
46. Rabiei F, Rahimi A R, Hadad M J, Saberi A. Experimental evaluation of coolant-lubricant properties of nanofluids in ultrasonic assistant MQL grinding. The International Journal of Advanced Manufacturing Technology, 2017, 93(9): 3935–3953
47. Yan L T, Zhang Q J, Yu J Z. Effects of continuous minimum quantity lubrication with ultrasonic vibration in turning of titanium alloy. The International Journal of Advanced Manufacturing Technology, 2018, 98(1): 827–837
48. Gao T, Zhang Y B, Li C H, Wang Y Q, An Q L, Liu B, Said Z, Sharma S. Grindability of carbon fiber reinforced polymer using CNT biological lubricant. Scientific Reports, 2021, 11(1): 22535
49. Jiang J L, Ge P Q, Sun S F, Wang D X, Wang Y L, Yang Y. From the microscopic interaction mechanism to the grinding temperature field: an integrated modelling on the grinding process. International Journal of Machine Tools and Manufacture, 2016, 110: 27–42
50. Sugita N, Ishii K, Sui J B, Terashima M. Multi-grooved cutting tool to reduce cutting force and temperature during bone machining. CIRP Annals, 2014, 63(1): 101–104
51. Babbar A, Jain V, Gupta D, Agrawal D, Prakash C, Singh S, Wu L Y L, Zheng H Y, Królczyk G, Bogdan-Chudy M. Experimental analysis of wear and multi-shape burr loading during neurosurgical bone grinding. Journal of Materials Research and Technology, 2021, 12: 15–28
52. Yang M, Li C H, Zhang Y B, Wang Y G, Li B K, Jia D Z, Hou Y L, Li R Z. Research on microscale skull grinding temperature field under different cooling conditions. Applied Thermal Engineering, 2017, 126: 525–537
53. Zhang J H, Zhao Y, Zhang S, Tian F Q, Guo L S, Dai R Z. Study on effect of ultrasonic vibration on grinding force and surface quality in ultrasonic assisted micro end grinding of silica glass. Shock and Vibration, 2014, 2014: 418059
54. Qu S S, Yao P, Gong Y D, Yang Y Y, Chu D K, Zhu Q S. Modelling and grinding characteristics of unidirectional C-SiCs. Ceramics International, 2022, 48(6): 8314–8324
55. Sun Y, Jin L Y, Gong Y D, Wen X L, Yin G Q, Wen Q, Tang B J. Experimental evaluation of surface generation and force time-varying characteristics of curvilinear grooved micro end mills fabricated by EDM. Journal of Manufacturing Processes, 2022, 73: 799–814
56. Liao Z R, Axinte D A. On chip formation mechanism in orthogonal cutting of bone. International Journal of Machine Tools and Manufacture, 2016, 102: 41–55
57. Jia D Z, Li C H, Zhang Y B, Yang M, Cao H J, Liu B, Zhou Z M. Grinding performance and surface morphology evaluation of titanium alloy using electric traction bio micro lubricant. Journal of Mechanical Engineering, 2022, 58(5): 198–211
58. Ding W F, Xu J H, Chen Z Z, Su H H, Fu Y C. Grindability and surface integrity of cast nickel-based superalloy in creep feed grinding with brazed CBN abrasive wheels. Chinese Journal of Aeronautics, 2010, 23(4): 501–510
59. Shu L M, Sugita N. Analysis of fracture, force, and temperature in orthogonal elliptical vibration-assisted bone cutting. Journal of the Mechanical Behavior of Biomedical Materials, 2020, 103: 103599
60. Brehl D E, Dow T A. Review of vibration-assisted machining. Precision Engineering, 2008, 32(3): 153–172
61. Gu P, Zhu C M, Tao Z, Yu Y Q. A grinding force prediction model for SiCp/Al composite based on single-abrasive-grain grinding. The International Journal of Advanced Manufacturing Technology, 2020, 109: 1563–1581
62. Zhou M, Zheng W. A model for grinding forces prediction in ultrasonic vibration assisted grinding of SiCp/Al composites. The International Journal of Advanced Manufacturing Technology, 2016, 87(9): 3211–3224
63. McCarus S D. Physiologic mechanism of the ultrasonically activated scalpel. Journal of the American Association of Gynecologic Laparoscopists, 1996, 3(4): 601–608
64. Wang Y, Lin B, Wang S L, Cao X Y. Study on the system matching of ultrasonic vibration assisted grinding for hard and brittle materials processing. International Journal of Machine Tools and Manufacture, 2014, 77: 66–73
65. Ying Z Z, Shu L M, Sugita N. Experimental and finite element analysis of force and temperature in ultrasonic vibration assisted bone cutting. Annals of Biomedical Engineering, 2020, 48(4): 1281–1290
66. Bai X F, Hou S J, Li K, Qu Y, Zhu W. Analysis of machining process and thermal conditions during vibration-assisted cortical bone drilling based on generated bone chip morphologies. Medical Engineering & Physics, 2020, 83: 73–81
67. Xie H M, Jiang B, He J J, Xia X S, Pan F S. Lubrication performance of MoS_2 and SiO_2 nanoparticles as lubricant additives in magnesium alloy-steel contacts. Tribology International, 2016, 93: 63–70